Competing reactions of selected atmospheric gases on Fe$_3$O$_4$ nanoparticles surfaces

Nermin Eltouny[a] and Parisa A. Ariya[a,b*]

[a]Department of Chemistry, McGill University

[b]Department of Atmospheric and Oceanic Sciences, McGill University, Montreal

801 Sherbrooke West, Montreal, QC, Canada H3A 2K6

*Corresponding author email: parisa.ariya@mcgill.ca

Supporting Information

X-ray diffraction (XRD)

Details on instrumental conditions for data collection acquired on a Siemens D5000 diffractometer with Cu Kα radiation ($\lambda = 1.5418$ Å) are presented in Table S1.

Table S1.   XRD data acquisition parameters for Fe$_3$O$_4$ NPs

XRD parameters	$2\theta(°)$	$\Delta 2\theta$ (°)	Δt(sec)
S$_{adsorption}$	20-70	0.5	10
S$_{reduced}$	10-70	0.5	10
S$_{oxidized}$	10-70	0.1	10

Analyses by GC-MS and GC-FID of a typical flask consisting of toluene and NO$_2$

The GC-MS spectra in Figure S1 show that the blanks for the flasks, with only dry air, contained peaks at retention times of 9.31 min (m/z = 73, 267, 268, 355, 356- cyclopentasiloxane) and 11.94 min (m/z = 73, 147, 251, 341, 429-cyclohexasiloxane) attributed to organosiloxanes. Organosiloxanes are due to the deactivating agent (Glassclad 18, UCT) used to coat the glassware. The organosiloxane peaks remained constant for the blank (dry air only), toluene and toluene + NO$_2$ flasks indicating that a reaction had not occurred with either the toluene or the NO$_2$. The CAR/PDMS SPME fibre consists of a fused silica fibre coated with PDMS in which porous carbon particles are embedded rendering it suitable for the sampling of volatile organic compounds [1]. including aldehydes, ketones and carboxylic acids [2]. Organics were not detected in the blank flasks within the detection limits of the SPME (low ppbv) and GC-MS; therefore it is unlikely that organic residues were left on the walls of the flasks in quantities sufficient to impact the reaction.
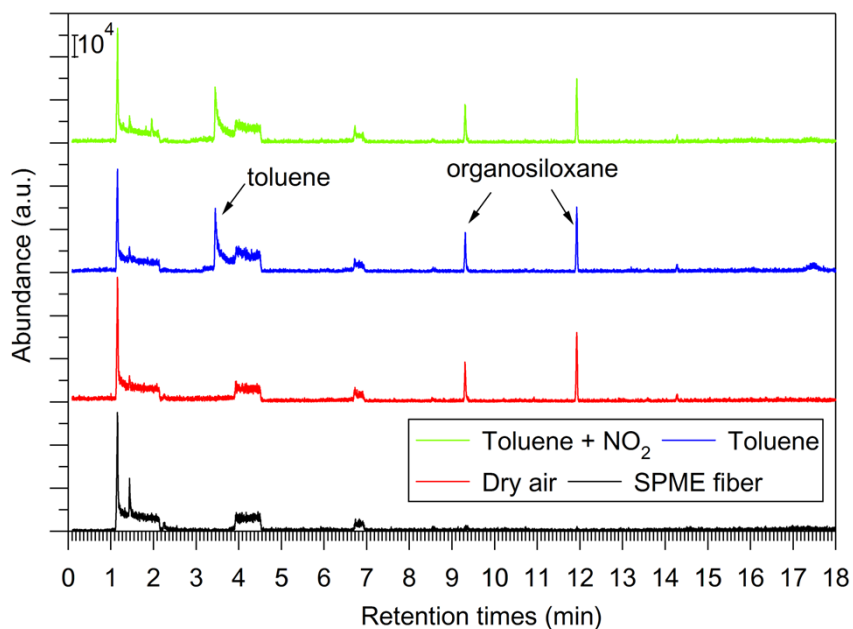

Figure S1.   Overlay of blank SPME fibre, blank flask containing dry air, flask containing toluene and flask containing toluene + NO$_2$.

Data acquisition using gas chromatography and solid phase micro-extraction (spme)

The initial GC-FID oven temperature was 50 °C; then a ramp rate of 20 °C.min^{-1} was applied and the temperature reached 110 °C, which was held for 2.2 minutes. Sampling was achieved using SPME with an extraction time of *c.a.,* 1 minute, which was injected in the GC port at 290 °C for 3 minutes. For the GC-MS data acquisition, the same temperature program was applied with the exception of the higher final temperature, which was set at 220 °C.

XPS spectra curve fitting and peak assignments

The Avantage Software (Thermo scientific) was used to deconvolute the high resolution spectra for Fe2p, C1s, and O1s core lines. Shirley and SMART backgrounds were subtracted from the C1s and O1s, and from the Fe2p, respectively. All spectra were charge corrected relative to adventitious carbon at 285.0 eV.[3] Peaks below 285.0 eV account for differential charging across the sample. The C1s spectra for $S_{reduced}$ and $S_{oxidized}$ are shown in Figure S1 and S2, respectively.
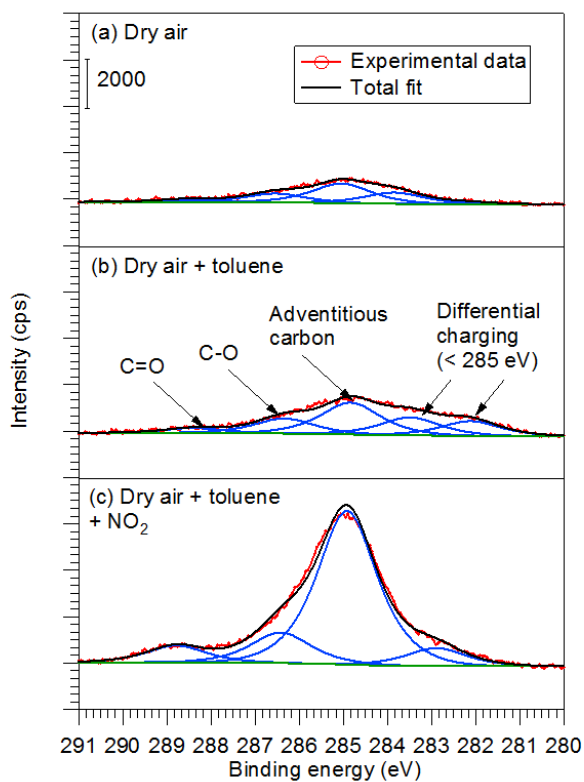
Figure S2. XPS C1s spectra for $S_{reduced}$.
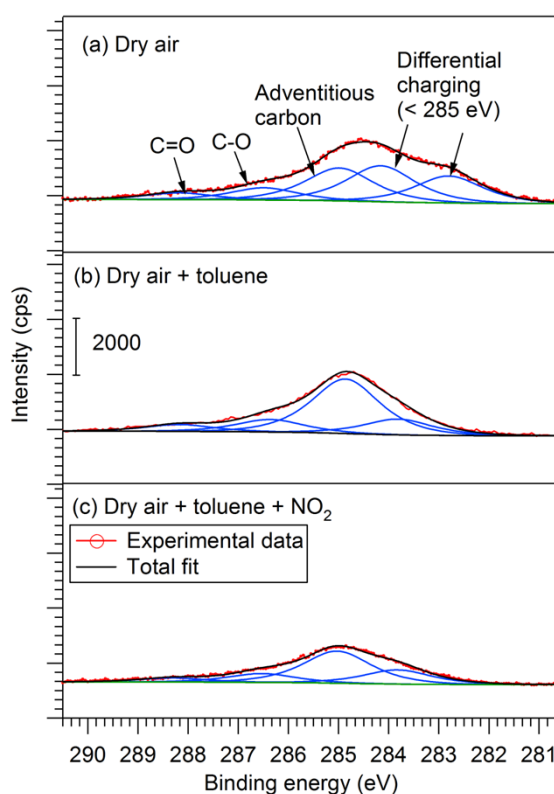
Figure S3. XPS C1s spectra for $S_{oxidized}$.

The $Fe2p_{3/2}$ spectra were deconvoluted into 5 peaks corresponding to one peak for Fe^{2+} (octahedral), and two peaks for Fe^{3+} (octahedral and tetrahedral), and two satellite peaks for Fe^{2+} and Fe^{3+} fixed at + 5.9 and 8.0 eV, respectively, which compare well with the reported value of 6.0 eV[4] and 8.0 eV.[4] To validate the fitted peaks, the atomic percent contributions of carbon-oxygen contributions in the C1s spectra were compared with those observed in the organic oxygen-carbon components of the O1s spectra, while the Fe^{2+} and Fe^{3+} contributions in the $Fe2p_{3/2}$ spectra were compared with those assigned to O-Fe and HO-Fe components of the O1s spectra. An example of element corroboration is given in Table S2. The full width half maxima for the fitted peaks of C1s, O1s, and Fe2p were fixed at 1.6 eV, 1.8 eV, and 3.4 eV, respectively, and are based on values determined in a previous study carried

out on the same instrument.[5] The L:G mixing ratios for curve fitted peaks were fixed at 40. For the purpose of clarity in the figures 5 and 7, the corresponding $Fe2p_{1/2}$ doublet for each fitted peak of the $Fe2p_{3/2,}$ arising from spin-orbit splitting and appearing above 718.7 eV are not labelled. Atomic percent contributions are calculated from the fitted peaks of $Fe2p_{3/2}$ due to the larger intensity ($Fe2p_{3/2}:Fe2p_{1/2}$ is 2:1).

Table S2.   XPS peak fittings for C1s, O1s, and $Fe2p_{3/2}$ spectra for $S_{oxidized}$ fraction (c) toluene + NO_2

Element Peak Deconvolution	Binding Energy (eV)	FWHM (eV)	Atomic %
Carbon: C1s			
Differential charging	283.8	1.6	4.2
C-C	285.0	1.6	9.5
C-O	286.5	1.6	2.6
C=O	288.3	1.6	1.21
Carbon-Oxygen contributions: 2.6+1.2 = 3.8 %			
Oxygen: O1s			
Nonequivalent oxygen	528.1	1.8	0.6
O-Fe	529.9	1.8	35.7
HO-Fe	531.4	1.8	8.9
O-C	533.3	1.8	2.9
Oxygen-Carbon contributions: 2.9 %			
Oxygen-Iron contribution = 35.7 + 8.9 = 44.6%			
Iron: $Fe2p_{3/2}$			
Fe^{2+} (oct)	710.06	3.4	8.5
Fe^{3+} (oct)	710.66	3.4	10.0
Fe^{3+} (thd)	713.46	3.4	5.9
Fe^{2+} Satellite	716.06	5.3	1.7
Fe^{3+} Satellite	718.7	5.3	8.0
Iron-Oxygen contributions:			
Fe-O = 8.5+1.7 = 10.2			
Fe_2O_3 = 10+5.9+8 = 24			
Fe-O total contribution = 10.2 + 24*1.5 = 46.2 %			

Error calculation on ratios obtained from XPS and TOF SIMS

The error on the ratios from XPS were determined using the corrected area under each peak assigned to species i and j, A_i and A_j, calculated by the Avantage™ software[6] and given by equation S1:

$$A_i = \frac{I_i}{T(E_i)R_i E_i^n}$$

(S1)

Where I_i is the intensity for species i, the kinetic energy, E_i, instrument transmission function, $T(E_i)$, relative sensitivity factor, R_i, and escape depth component, n. The error, σR, is calculated using the method of propagation of errors[7] using equation S2, :

$$\sigma R = R \sqrt{\left(\frac{\sigma A_i}{A_i}\right)^2 + \left(\frac{\sigma A_j}{A_j}\right)^2}$$

(S2)

where $\sigma A_{i,j}$ is the square root of A_i. The errors on the ratios from TOF SIMS were calculated using the equation S2 and by replacing the area with ion intensity.

Examples of other adsorption experiments
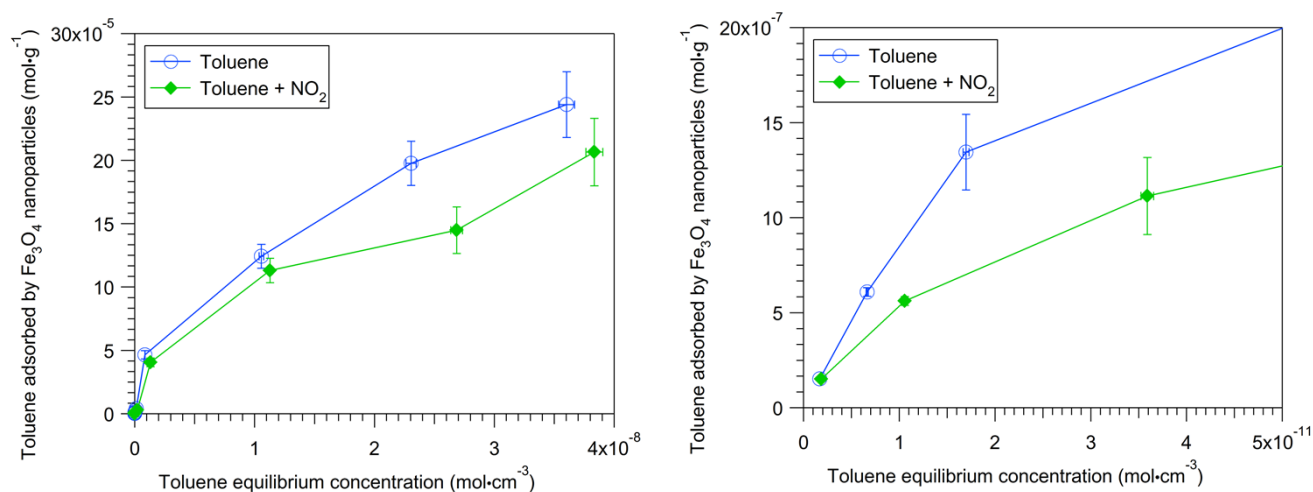
Figure S4. Experimental adsorption isotherms of toluene on Fe_3O_4 NPs NPs in dry air alone and in the presence of NO_2 at the low (left graph) and high (right graph) concentration range.

Figure S5. Experimental adsorption isotherms of toluene on Fe_3O_4 NPs NPs in dry air alone and in the presence of NO_2 at the low (left graph) and high (right) concentration range. Error bars represent standard errors calculated by the propagation of error during preparation and analyses.

Table S3.   Adsorption models and their respective assumptions
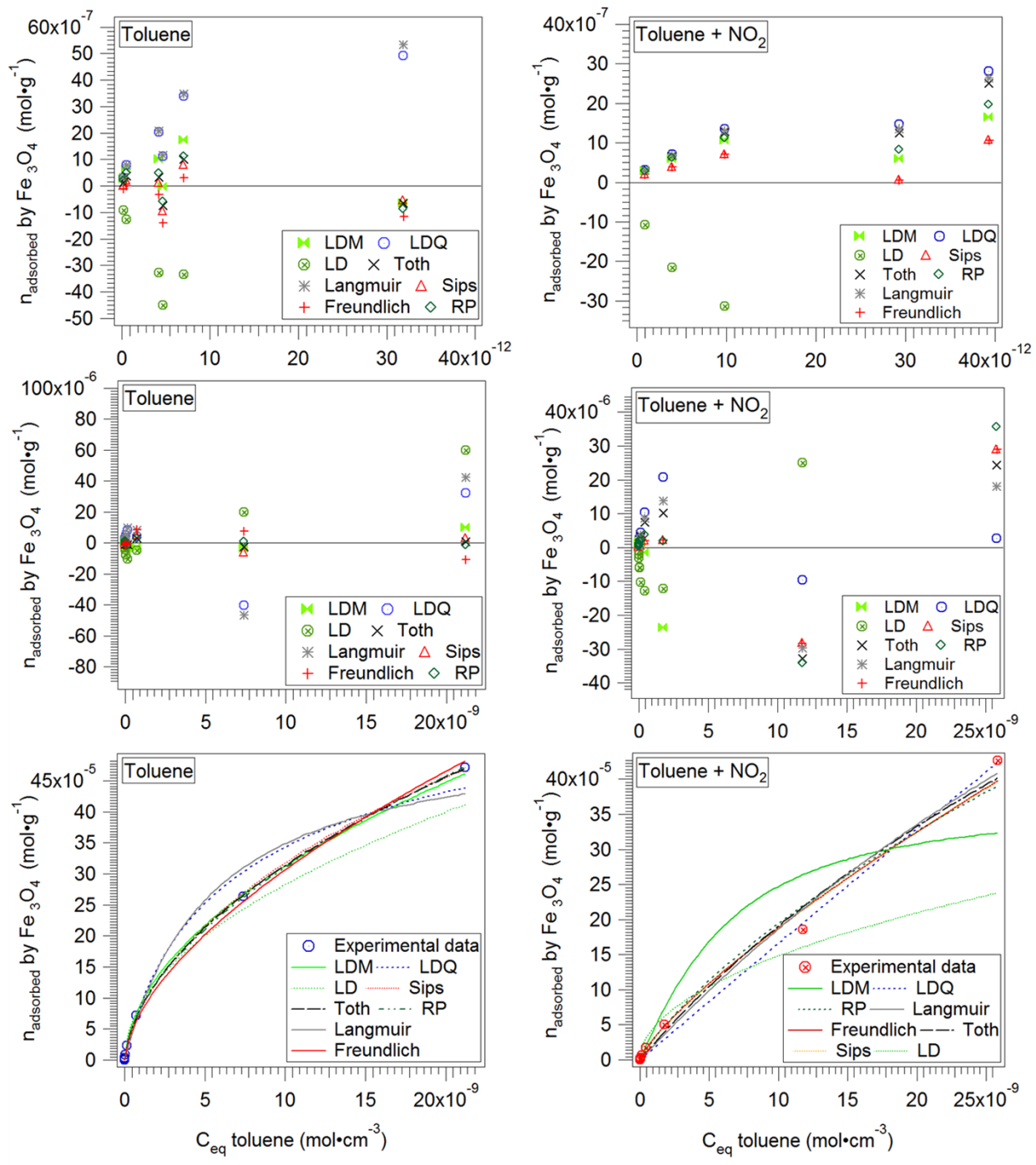
Model	Equation	Parameter description	Applicability/Assumptions
Langmuir[8]	$n_{ads} = q_m \dfrac{bC_{eq}}{1+bC_{eq}}, b = \dfrac{s_0 e^{\frac{q_{st}}{kT}}}{v\sigma\sqrt{2\pi mkT}}$	q_m: monolayer adsorption capacity, s_0: initial sticking probability q_{st}: isosteric heat of adsorption σ: density of adsorption sites v: frequency factor	Homogeneous energy sites[9] No lateral interaction
Freundlich[10]	$n_{ads} = K_F C_{eq}^{\frac{1}{n}}$	K_F: Freundlich constant n: heterogeneity parameter	Heterogeneity of energy sites No lateral interactions
Toth[11]	$n_{ads} = q_m \dfrac{QtC_{eq}}{\left(Kt + C_{eq}^{t}\right)^{1/t}}$	Qt and Kt: Toth constants t: heterogeneity parameter[12] (0-1)	Heterogeneity of sites,[9] lateral interactions Reduces to Langmuir[13] for t=1
Redlich- Peterson (RP)[14]	$n_{ads} = \dfrac{K_r C_{eq}}{\left(1 + A_r C_{eq}^{g}\right)}$	Kr and Ar: RP constants b: 0-1	Homogeneous and heterogeneous Reduces to Freundlich at high Ceq [15]
Sips	$n_{ads} = \dfrac{K_s A_s C_{eq}^{S}}{\left(1 + A_s C_{eq}^{S}\right)}$	Ks: max ads cap As: Sips constant s: isotherm exponent (-1-+1)	Heterogeneous energy sites,[16] no lateral interaction Reduces to Langmuir at high Ceq[17] Reduces to Freundlich at low Ceq[18]
Langmuir Dissociative adsorption (LD)[19]	$n_{ads} = q_m \dfrac{\sqrt{b_2 C_{eq}}}{1 + \sqrt{b_2 C_{eq}}}, b_2 = \dfrac{s_0 e^{\frac{q_{st}}{kT}}}{v\sigma^2\sqrt{2\pi mkT}}$		Recombinative 2nd desorption Energetically heterogeneous sites present in equal concentration[19]
Langmuir Dissociative adsorption (LDQ)[19]	$n_{ads} = q_m \dfrac{1 + 2bC_{eq} - \sqrt{1 + 4bC_{eq}}}{2bC_{eq}}$		Quasi 1st order desorption-dissociated species are immobile
Langmuir Dissociative and mobile adsorption (LDM)[19]	$q = q_m \dfrac{1 + bC_{eq} - \sqrt{[1 - bC_{eq}]^2 + 4KbC_{eq}}}{2(1 - K)}$	$p_d{}'$: desorption probability at occupied site p_d: desorption probability at unoccupied site	Mobile adsorption

$$K = \frac{p_d'}{p_a + p_d}$$

p_a: adsorption probability

Table S4. Fitting parameters for adsorption models of the adsorption of toluene on Fe_3O_4 NPs with and without NO_2 in air.

Isotherm model: RP, LD, LDQ, LDM

Toluene

	RP			LD		LDQ		LDM		
	K_r (×10⁵)	A_r	g (×10⁻¹)	b	Q_m (×10⁻¹)	b (×10⁸)	Q_m (×10⁻⁴)	b (×10⁶)	Q_m (×10⁻²)	K (×10³)
Values	8.6	1.2×10⁵	4.6	732	1.05	1.45	7.7	2.38	8.0	5.65
ERR_{SD}	3.0	2.9×10⁴	0.21	0	0.082	0.178	0	0	0	0.235
Adj. R²	**0.998**			**0.947**		**0.975**		**0.997**		

Toluene, NO_2

	K_r (×10⁴)	A_r (×10³)	g	b	Q_m (×10⁻²)	b (×10⁵)	Q_m (×10⁻²)	b (×10⁸)	Q_m (×10⁻⁴)	K (×10⁻¹)
Value	4.3	4.6	0.45	437	7.10	4.20	3.99	1.33	1.0	4.76
ERR_{SD}	1.3	2.4	0	0	1.31	0.08	0	0	0	3.2
Adj. R²	**0.977**			**0.764**		**0.996**		**0.899**		

Isotherm model: Freundlich, Langmuir, Toth, Sips

Toluene

	Freundlich		Langmuir		Toth			Sips		
	K_F	n (×10⁻²)	b (×10⁸)	Q_m (×10⁻⁴)	Q_t	K_t	t (×10⁻²)	K_s (×10⁻³)	A_s (×10⁴)	S (×10⁻²)
Values	20.1	166	1.83	5.39	0.918	0.194	9.92	1.86	3.37	65.2
ERR_{SD}	4.57	3.28	0.619	0.738	2.68	0.130	3.20	0.550	2.49	2.21
Adj. R²	**0.996**		**0.963**		**0.998**			**0.998**		

Toluene, NO_2

	K_F (×10²)	n (×10⁻²)	b (×10⁷)	Q_m (×10⁻³)	Q_t (×10⁻³)	K_t (×10⁻⁵)	t	K_s	A_s	S (×10⁻²)
Value	3.75	127	1.29	1.63	2.50	1.12	0.718	1.43	2.65 × 10²	78.8
ERR_{SD}	2.23	5.15	1.16	1.19	1.80	0.740	0	1.37 × 10³	2.54 × 10⁵	8.18
Adj. R²	**0.987**		**0.965**		**0.969**			**0.986**		

Figure S6. Comparison of isotherms (bottom) fitted using different models and respective residuals over low (top) and high (middle) concentration range for the adsorption of toluene on Fe$_3$O$_4$ NPs with (right) and without NO$_2$ (left) in air.

Details on the calculations used in the Akaike criterion test for the comparison of adsorption models

The small-sample corrected AIC values for each model are calculated according to equation 1 and the relative likelihood of the model with lower AIC value is calculated using equation 2 (OriginPro 8® [20])

$$AIC = Nln\left(\frac{RSS}{N}\right) + 2K + \frac{2K(K+1)}{N-K-1}, where \frac{N}{K} < 40 \quad (1)$$

$$Relative\ likehood = \exp\left(-\frac{1}{2}\Delta i\right), where\ \Delta i = abs(AIC(RP)) - abs(AIC\ (F)) \quad (2)$$

TOF SIMS spectra
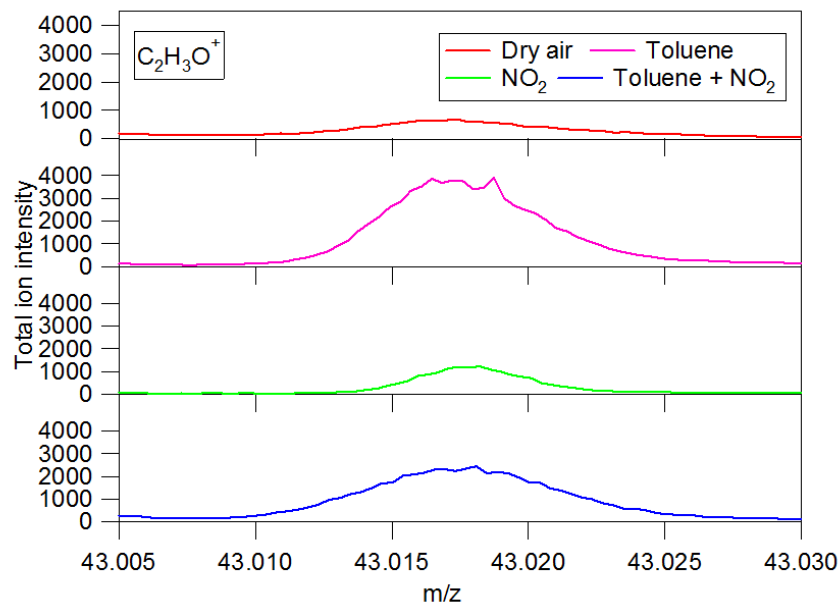
Figure S7. Positive mode TOF SIMS m/z 43 total ion intensities for fractions of Fe_3O_4 NPs batch $S_{oxidized}$
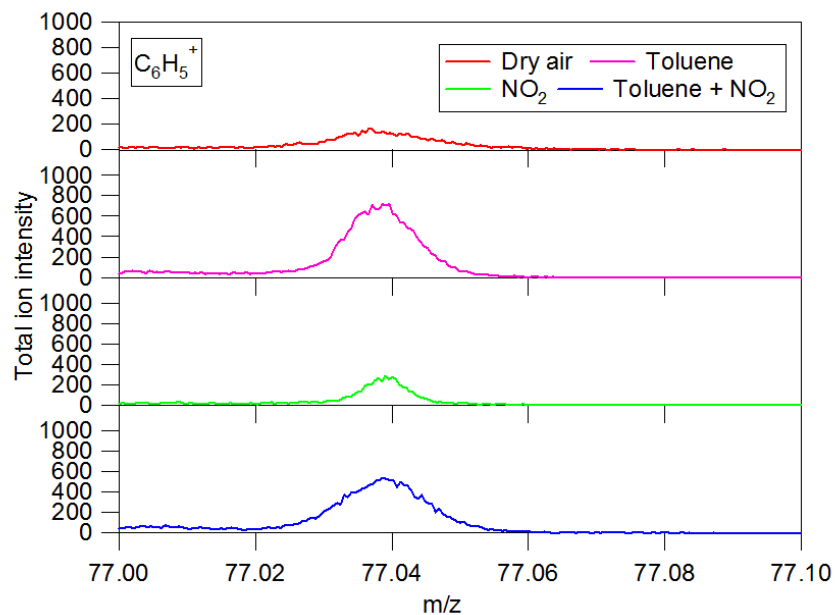
Figure S8. Positive mode TOF SIMS m/z 77 total ion intensities for fractions of Fe_3O_4 NPs batch $S_{oxidized}$
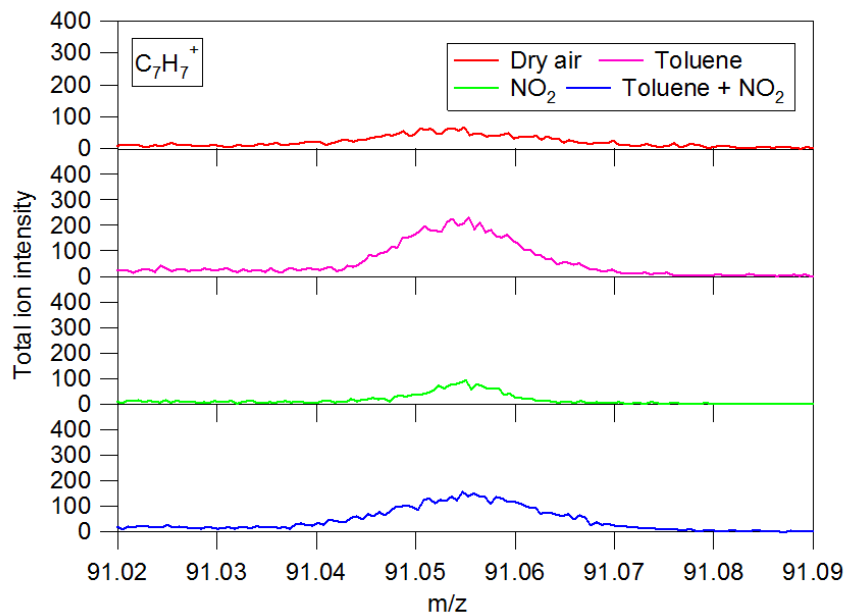
Figure S9. Positive mode TOF SIMS m/z 91 total ion intensities for fractions of Fe_3O_4 NPs batch $S_{oxidized}$

Figure S10. Positive mode TOF SIMS m/z 105 total ion intensities for fractions of Fe_3O_4 NPs batch $S_{oxidized}$.

Table S5.   Assignments of binding energies (in eV) and ratios calculated from high resolution fitted spectra of Fe2p and O1s XPS for Fe_3O_4 NPs exposed to 0.65 ppmv of NO_2 alone in dry air.

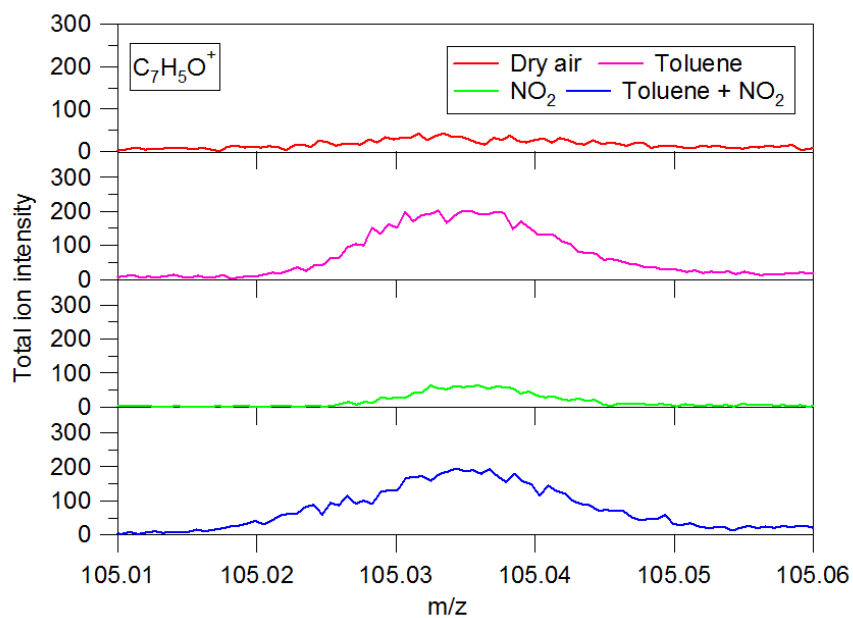| Assigned Species, Reported literature BE	$S_{oxidized}$ NO_2
OH (nonequivalent):-1.6, O^{2-} (undercoordinated):-1 (rel. Fe-O) [21]	527.6
O-Fe: 529.9 ± 0.4[5], 530.1 ± 0.2 [4]	530.1
HO-Fe, Adsorbed O, O=C: 531.4 ± 0.2 [4], 531.6 [22], 531.3 531.9-532.8 [23]	531.6
NO_3 /NO_2 (on TiO_2):532.5/533 [24] O-C: 532.4-533.5 [23]	
H_2O on Fe_3O_4: 532.7 ± 0.1 γ-Fe_2O_3 : 533.3 ± 0.1 [25], H_2O: 534 [21]	533.2
Fe^{2+}/Fe^{3+}	0.31 ± 2.2 × 10^{-2}
Fe/O	0.60 ± 2.2 ×10^{-2}
O > 531.2 eV /O (total)	0.12 ± 8.3 × 10^{-3}
O > 531.2 eV /Fe-O (non equiv., FeOH and FeO)	0.13 ± 8.8 × 10^{-3}
FeOH (including peak at 528 eV)/ FeO	0.35 ± 2.0 × 10^{-2}

Gas phase qualitative and quantitative analyses by GC-MS and GC-FID for flasks containing toluene and NO_2 only

To ensure that gas phase reactions between toluene and NO_2 did not occur, the gas phase was analyzed with GC-MS and GC-FID for the two systems (toluene and toluene + NO_2). The GC-MS chromatograms in Figure S1 show that new peaks do not form when NO_2 is added to the system. We quantified the toluene concentration using the GC-FID detection system because it is more accurate than the GC-MS (run in Scan mode). In the absence of NPs, the peak area of toluene detected should be proportional to the concentration of toluene (amount of toluene injected in the flask). The difference between the concentrations of toluene alone and in the presence of NO_2 is within the allowable error of uncertainty (10 %). The linear fits show that the slopes for both systems are within the 10% uncertainty. These results indicate that toluene does not react with NO_2 in the gas phase under our experimental conditions, outside the margin of instrumental uncertainties. If a reaction had occurred in a significant manner, a decrease in the concentration of toluene would have been expected and new peaks detected, which is not the case.

A note on experimental uncertainties on Fe^{2+}/Fe^{3+} ratios in XPS studies

XPS experiments for the adsorption of toluene to magnetite NPs of in dry air show a change in the Fe^{2+}/Fe^{3+} ratio that is within experimental uncertainties, i.e., ± 0.02. We have systematically observed[26] an increase in the Fe^{2+}/ $Fe^{3,}$ for this specific system constituted of toluene, dry air and Fe_3O_4 NPs [+]. The sample $S_{oxidized}$ exposed to 100 ppmv of toluene only in dry air reveals the same increasing trend in the Fe^{2+}/Fe^{3+}. Therefore, this increase is likely real albeit small when compared to samples tested in our

previous study shown in the figure below. It is possible that the change is not as high as what was observed for other samples due to the higher initial oxidation level of $S_{reduced}$, which is closest to the stoichiometric ratio value of 0.50 for Fe_3O_4.

References

(1)   Mani, V. In *Applications of Solid Phase Microextraction*; Pawliszyn, J., Ed.; The Royal Society of Chemistry: 1999, p 57.

(2)   Natera Marín, R.; Castro Mejías, R.; de Valme García Moreno, M.; García Rowe, F.; García Barroso, C. *Journal of Chromatography A* **2002**, *967*, 261.

(3)   Briggs, D. *Handbook of x-ray and ultraviolet photoelectron spectroscopy*; Heyden: London; Philadelphia, 1977.

(4)   Mills, P.; Sullivan, J. L. *J. Phys. D: Appl. Phys.* **1983**, *16*, 723.

(5)   Poulin, S.; França, R.; Moreau-Bélanger, L.; Sacher, E. *J. Phys. Chem. C* **2010**, *114*, 10711.

(6)   Thermo Fischer Scientific Inc.; Thermo Fischer Scientific Inc: 2013.

(7)   Taylor, J. R. *An introduction to error analysis : the study of uncertainties in physical measurements*; University Science Books: Mill Valley, Calif., 1982.

(8)   Langmuir, I. *J. Amer. Chem. Soc.* **1918**, *40*, 1361.

(9)   Dąbrowski, A. *Adv. Colloid Interface Sci.* **2001**, *93*, 135.

(10)   Freundlich, H. *Trans. Faraday Soc.* **1932**, *28*, 195.

(11)   Rudzinski, W.; Everett, D. H. *Adsorption of gases on heterogeneous surfaces*; Access Online via Elsevier, 1991.

(12)   Tóth, J. *Adv. Colloid Interface Sci.* **1995**, *55*, 1.

(13)   Kim, J.-H.; Lee, S.-J.; Kim, M.-B.; Lee, J.-J.; Lee, C.-H. *Industrial & Engineering Chemistry Research* **2007**, *46*, 4584.

(14)   Redlich, O.; Peterson, D. L. *J. Phys. Chem.* **1959**, *63*, 1024.

(15)   Jossens, L.; Prausnitz, J. M.; Fritz, W.; Schlünder, E. U.; Myers, A. L. *Chem. Eng. Sci.* **1978**, *33*, 1097.

(16)   Jaroniec, M. *Surf. Sci.* **1975**, *50*, 553.

(17)   Foo, K. Y.; Hameed, B. H. *Chem. Eng. J.* **2010**, *156*, 2.

(18)   Sips, R. *J. Chem. Phys.* **1950**, *18*, 1024.

(19)   Ranke, W.; Joseph, Y. *Phys. Chem. Chem. Phys.* **2002**, *4*, 2483.

(20)   OriginLab Corporation.

(21)   Kendelewicz, T.; Kaya, S.; Newberg, J. T.; Bluhm, H.; Mulakaluri, N.; Moritz, W.; Scheffler, M.; Nilsson, A.; Pentcheva, R.; Brown, G. E. *J. Phys. Chem. C* **2013**, *117*, 2719.

(22)   Grosvenor, A. P.; Kobe, B. A.; McIntyre, N. S. *Surf. Sci.* **2004**, *565*, 151.

(23)   Beamson, G. B. D. *High resolution XPS of organic polymers : the Scienta ESCA300 database*; Wiley: Chichester [England]; New York, 1992.

(24)   Haubrich, J.; Quiller, R. G.; Benz, L.; Liu, Z.; Friend, C. M. *Langmuir* **2010**, *26*, 2445.

(25)   Biesinger, M. C.; Payne, B. P.; Grosvenor, A. P.; Lau, L. W. M.; Gerson, A. R.; Smart, R. S. C. *Appl. Surf. Sci.* **2011**, *257*, 2717.

(26)   Eltouny, N. A.; Ariya, P. A. *Ind. Eng. Chem. Res.* **2012**, *51*, 12787.